LIMNOLOGY
and
OCEANOGRAPHY

ASLO

Limnol. Oceanogr. 64, 2019, 1980–1995

doi: 10.1002/lno.11164

Ecophysiology of mesophotic reef-building corals in Hawai'i is influenced by symbiont–host associations, photoacclimatization, trophic plasticity, and adaptation

Jacqueline L. Padilla-Gamiño,[1]* Melissa S. Roth,[2] Lisa J. Rodrigues,[3] Christina J. Bradley,[4] Robert R. Bidigare,[5] Ruth D. Gates,[5] Celia M. Smith,[6] Heather L. Spalding[6]

[1]School of Aquatic and Fishery Sciences, University of Washington, Seattle, Washington
[2]Department of Plant and Microbial Biology, University of California, Berkeley, Berkeley, California
[3]Department of Geography and the Environment, Villanova University, Villanova, Pennsylvania
[4]Department of Biological Sciences, Salisbury University, Salisbury, Maryland
[5]Hawai'i Institute of Marine Biology, University of Hawaii, Kāneohe, Hawai'i
[6]Department of Biology, College of Charleston, Charleston, South Carolina

Abstract

Mesophotic reef corals remain largely unexplored in terms of the genetic adaptations and physiological mechanisms to acquire, allocate, and use energy for survival and reproduction. In the Hawaiian Archipelago, the *Leptoseris* species complex form the most spatially extensive mesophotic coral ecosystem known and provide habitat for a unique community. To study how the ecophysiology of *Leptoseris* species relates to symbiont–host specialization and understand the mechanisms responsible for coral energy acquisition in extreme low light environments, we examined *Symbiodinium* (endosymbiotic dinoflagellate) photobiological characteristics and the lipids and isotopic signatures from *Symbiodinium* and coral hosts over a depth-dependent light gradient (55–7 μmol photons m^{-2} s^{-1}, 60–132 m). Clear performance differences demonstrate different photoadaptation and photoacclimatization across this genus. Our results also show that flexibility in photoacclimatization depends primarily on *Symbiodinium* type. Colonies harboring *Symbiodinium* sp. *COI-2* showed significant increases in photosynthetic pigment content with increasing depth, whereas colonies harboring *Symbiodinium* spp. *COI-1* and *COI-3* showed variability in pigment composition, yield measurements for photosystem II, as well as size and density of *Symbiodinium* cells. Despite remarkable differences in photosynthetic adaptive strategies, there were no significant differences among lipids of *Leptoseris* species with depth. Finally, isotopic signatures of both host and *Symbiodinium* changed with depth, indicating that coral colonies acquired energy from different sources depending on depth. This study highlights the complexity in physiological adaptations within this symbiosis and the different strategies used by closely related mesophotic species to diversify energy acquisition and to successfully establish and compete in extreme light-limited environments.

Light availability is a crucial factor affecting the physiology, productivity, distribution, and abundance of life in the ocean (Gattuso et al. 2006; Falkowski and Raven 2007). Both quantity and quality (spectral composition) of photosynthetically active radiation (PAR) can influence the recruitment, physiological performance, and survival of different life stages of marine organisms (Mundy and Babcock 1998; Falkowski and Raven 2007; Roth 2014). As depth increases, light intensity not only decreases exponentially but also ultraviolet and red wavelengths decrease faster causing a spectral enrichment in the blue and blue–green wavelengths (Kirk 2011). Scleractinian corals are ecologically and economically important organisms that live in a mutualistic symbiosis with intracellular algae (dinoflagellates of the genus *Symbiodinium*) and depend on PAR to obtain energy for photosynthesis. *Symbiodinium* translocate fixed carbon to their coral host to meet their host's metabolic demands as well as contribute to coral growth and calcification (Goreau and Goreau 1959; Muscatine 1990). Most symbiotic

*Correspondence: jpgamino@uw.edu

Additional Supporting Information may be found in the online version of this article.

This manuscript is dedicated to the memory of our dearest Ruth Gates, an incredible scientist, mentor, and friend. We deeply miss you.

corals cannot photosynthesize and survive at depths greater than 60 m as PAR availability is limited in spectral features and quantity (Fricke et al. 1987; Lesser et al. 2009; Loya et al. 2016). However, some species persist and even flourish in dimly lit environments such as the mesophotic zone, where downwelling irradiance can be as low as 1% of surface irradiance (Kahng and Kelley 2007; Lesser et al. 2009; Bridge et al. 2011; Pyle et al. 2016). Mesophotic coral ecosystems, as currently defined, are deep fore-reef communities comprised largely of light-dependent zooxanthellate corals, azoxanthellate scleractinian corals, macroalgae as well as sponges from 30 m to over 150 m depths (Lesser et al. 2009; Hinderstein et al. 2010; Baker and Harris 2016). Upper mesophotic coral reefs inhabit depths from 30 to 60 m, whereas lower mesophotic reefs are present from 60 to 150 m depths. To date, mesophotic reef corals remain largely unexplored in terms of the physiological adaptations and mechanisms that allow resident species to live and successfully reproduce in these environments (Lesser et al. 2010; Shlesinger et al. 2018). However, it is important to study mesophotic reefs because of the fundamentally new scientific insights these environments can provide and their potential to serve as refuges and nursery habitats for many ecologically and commercially important species (Riegl and Piller 2003; Lesser et al. 2009; Bongaerts et al. 2010; Bryan et al. 2013; Holstein et al. 2016).

Light-dependent corals are important members of the mesophotic community (Lesser et al. 2009). *Leptoseris* is a common obligate zooxanthellate genus found in mesophotic environments around the world including the Pacific Ocean, Red Sea, and the Caribbean Sea (Bouchon 1981; Fricke and Knauer 1986; Maragos and Jokiel 1986; Kahng and Maragos 2006; Ziegler et al. 2015). The deepest reported zooxanthellate species is *Leptoseris hawaiiensis*, which has been found as deep as 165 m depth at Johnston Atoll (Maragos and Jokiel 1986).

One of the most studied corals from the deep mesophotic zone is *Leptoseris fragilis* from the Red Sea. This species lives exclusively between 40 and 145 m depths (154–1.2 μmol photons m^{-2} s^{-1}; Fricke and Schuhmacher 1983; Fricke et al. 1987) and its success in the mesophotic zone has been attributed to its photophysiological flexibility, efficient use of low photon flux densities, and ability to switch between photoautotrophy and heterotrophy to meet its metabolic needs (Schlichter et al. 1985; Fricke et al. 1987; Schlichter 1991; Schlichter et al. 1997). However, the population genetics of *L. fragilis* host and *Symbiodinum* have not been studied and any physiological differences with depth are likely to reflect adaptations of different host species and/or *Symbiodinium* types. The Caribbean coral *Montastrea cavernosa* shows morphological and genetic differentiation across depths (Lesser et al. 2010; Brazeau et al. 2013), and displays physiological acclimatization and photoadaptation associated with different *Symbiodinium* composition between shallow (0–46 m) and greater depths (61–91 m). Furthermore, a shift from photoautotrophy to heterotrophy occurred between 45 and 61 m, and lower productivity was found at greater depths (Lesser et al. 2010).

Previous studies have found that both photobiological flexibility and *Symbiodinium* type are essential to persist in light-limited environments (Frade et al. 2008; Cooper et al. 2011; Ziegler et al. 2015). In the Caribbean, *Madracis* spp. showed photoacclimatization by varying *Symbiodinium* density and type, as well as efficiency of light harvesting across depths from 5 to 40 m (Frade et al. 2008). In Western Australia, *Pachyseris speciosa* and *Seriatopora hystrix* showed different patterns of host–*Symbiodinium* specialization across depths (0–60 m). *P. speciosa* hosted mainly *Symbiodinium* type C across its depth range (0–60 m), whereas *S. hystrix* hosted *Symbiodinium* type D1a at shallow depths (0–20 m) and *Symbiodinium* C type at deeper depths (10–45 m; Cooper et al. 2011). Interestingly, *S. hystrix* had an increase in metabolic costs when hosting *Symbiodinium* C compared to type D1a while exposed to higher irradiances, suggesting that metabolic demands may depend on *Symbiodinium* type (Hoadley et al. 2015; Leal et al. 2015; Pernice et al. 2015). In the Red Sea, *Symbiodinium* densities and ratios of photoprotective and photosynthetic pigments decreased with depth (0–60 m) in *Porites*, *Leptoseris*, *Pachyseris,* and *Podabacia*. *Porites* harbored *Symbiodinium* type C15 while *Pachyseris* and *Podabacia* hosted mainly *Symbiodnium* type C1 and had a more limited depth range (Ziegler et al. 2015). These studies underlie the importance of genotyping *Symbiodinium* when investigating coral physiology from different light regimes. Both adaptation (change in the genetic makeup of a population over multiple generations) and acclimatization (when an organism adjusts to a change in its environment) strategies can play an important role in an organism's survival when light becomes limited.

In Hawaiian waters, *Leptoseris* is the dominant coral genus in the mid to deep mesophotic zones (60–160 m) and colonies of *Leptoseris* species form the most spatially extensive mesophotic coral ecosystem documented to date (Costa et al. 2015; Veazey et al. 2016; Spalding et al. 2019). These reef-building corals form extensive reefs with up to 100% live coral cover predominantly at 90–100 m (Kahng and Kelley 2007; Rooney et al. 2010). Species of *Leptoseris* form large (> 1 m in diameter), thin-walled colonies with plating and foliaceous morphologies that can grow approximately 1 cm yr^{-1} (Kahng 2013; Pyle et al. 2016), comparable to some shallow water corals. In contrast, *L. fragilis* mesophotic colonies in the Red Sea grow ~ 0.2–0.8 mm yr^{-1} and have a maximum diameter of 8–10 cm (Fricke et al. 1987). Because of the significant role of *Leptoseris* corals in creating mesophotic environments, insight into their physiology is critical to understand the ecosystem.

Leptoseris reefs in Hawai'i are hotspots of biodiversity and productivity with significantly higher rates of endemism in fishes compared to shallow reefs (Rooney et al. 2010; Kane et al. 2014; Pyle et al. 2016). These reefs facilitate recruitment of other species (Supporting Information Fig. S1), may function as refuges for fishery-targeted species already impacted on shallow reefs (Lindfield et al. 2016), and are distinctive habitats that harbor many undescribed and unique species (Pyle et al. 2016; Spalding et al. 2016).

Recent morphological and molecular studies have addressed the high cryptic diversity in *Leptoseris* from Hawai'i, revealing new insights about the diversity and adaptation of *Leptoseris–Symbiodinium* associations in this light-limited environment (Luck et al. 2013; Pochon et al. 2015). Using the cox-1-rRNA intron and skeletal micromorphology, Luck et al. (2013) reported a depth zonation pattern for different *Leptoseris* clades. Using a similar molecular approach (cox-1-rRNA intron), Pochon et al. (2015) examined host–*Symbiodinium* relationships in *Leptoseris* finding five cryptic species and variation in associated *Symbiodinium* across depths. However, the physiological flexibility of these different assemblages or their success in meeting host metabolic demands at different depths remains unexamined. Kahng et al. (2012) attributed the success of *Leptoseris* in the mesophotic zone to a low level of reflectivity associated with microscale optical geometry of the coral skeleton. However, this hypothesis remains largely untested.

In this study, we used an integrative approach to explore the status and flexibility of photobiology and trophic ecology of mesophotic species in the *Leptoseris* genus. Specifically, we address the following questions: (i) What mechanisms enable the reef-building coral *Leptoseris* spp. to live in the mesophotic zone? (ii) Is the photobiology of *Leptoseris* influenced by host–*Symbiodinium* specialization? (iii) What are the strategies for energy acquisition from 60 to 130 m depths? An understanding of the physiological state and flexibility of these species is essential for characterizing the status and resilience of mesophotic reefs in Hawai'i.

Methods

Study site

Samples of cryptically diverse *Leptoseris* spp. were collected across multiple depths (60–130 m) in the 'Au'au Channel offshore of Olowalu, west Maui (20°46.851′N, 156°40.391′W), in April 2009, January 2010, and February and March 2011 using the *Pisces IV* and *Pisces V* submersibles, respectively (Fig. 1A; Supporting Information Table S1). The 'Au'au Channel (Fig. 1B) separates the islands of Maui and Lāna'i and has a bottom topography consisting of a gently sloping, continuous limestone bridge. Underwater irradiance was measured at six sites in areas with *Leptoseris* spp. reefs in the 'Au'au Channel and Maui Nui

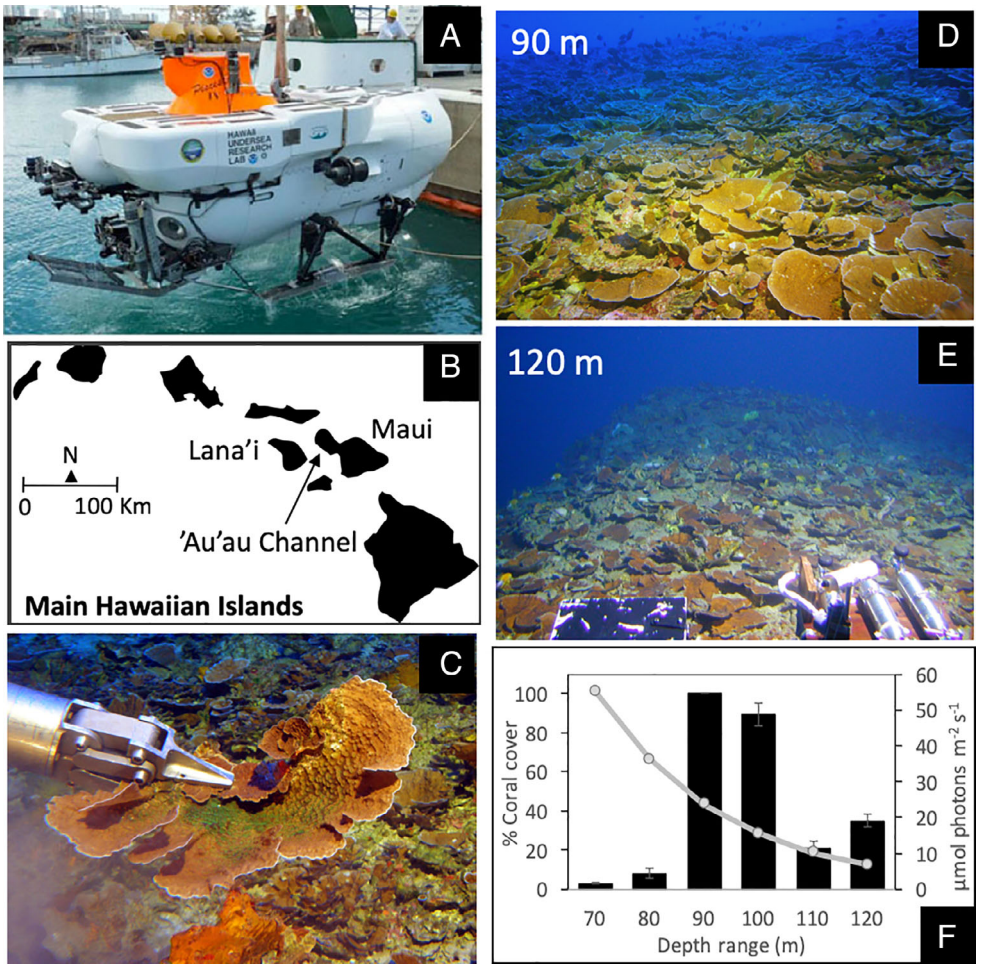

Fig. 1. (**A**) Submersible *Pisces IV*, (**B**) collection site in the 'Au'au Channel, Hawai'i, (**C**) Schilling Titan 4 manipulator arm collecting *Leptoseris* spp. sample, (**D**, **E**) *Leptoseris* reef at 90 and 120 m, and (**F**) coral cover (black bars) by depth plotted with PAR levels (gray line).

island complex during August 2008 and July 2010 (Supporting Information Table S2) to characterize the light environment. Irradiance was measured by lowering a calibrated spherical (4π) quantum sensor (Underwater LI-193SA, LI-COR©) through the water via a profiling rig; data were stored with a LI-COR© LI-1400 data logger. Scalar irradiance (E_0) is the best all-round measure of light availability for photosynthesis at a given depth, because photons are equally useful in photosynthesis regardless of their source direction (Kirk 2011). Furthermore, we observed *Symbiodinium* within coral cells on both the top and undersides of coral colonies, suggesting that irradiance from multiple directions could be used for photosynthesis. The sensor was attached to a 1-m-long arm mounted on a polyvinyl chloride housing to reduce instrument shading. The housing was integrated with a calibrated pressure transducer for depth (m) and a temperature sensor. PAR (in μmol photons m^{-2} s^{-1} from 400 to 700 nm) was recorded at known depths in the water column to maximum depths ranging from 64 to 94 m on calm, clear days (< 10% cloud cover) during midday (12:00–13:00 h). Furthermore, irradiance profiles were conducted on the sunny side of the vessel to reduce shadows. The vertical attenuation coefficient for scalar irradiance (K_0) from the downward portion of each profile was calculated according to the relationship in Beer's Law: $E_z = E_0 \times e^{-K0z}$ where z represents depth, E_z represents the intensity of irradiance at depth z, and E_0 represents the irradiance just beneath the surface (Kirk 2011). K_0 was then used to extrapolate irradiance at every 1 m depth for each profile, and an average irradiance profile (± SE) was calculated from six profiles. Optical depths for 1% and 10% surface irradiances were calculated using K_0 (Kirk 2011). In deep, clear, homogenous waters with little scattering and a diffuse light environment, the relationship of the vertical attenuation coefficients K_0 (scalar irradiance) and K_d (downwelling irradiance) is nearly one (Kirk 2011), thus allowing for a direct comparison between K_0 and K_d. Daily mid-day irradiance vertical profiles showed little stratification in the water column, with r^2 values ranging from 0.97 to 0.99 (Supporting Information Table S3). The vertical attenuation coefficients, K_0 (m^{-1}), ranged from –0.037 to –0.047 m^{-1}, with a mean K_0 (± SE) of –0.041 m^{-1} (± 0.001). The calculated mean optical depths, which correspond to the midpoint (10% surface irradiance) and the lower limit (1% surface irradiance) of the euphotic zone, were 56 and 112 m, respectively. This corresponded to a decrease in irradiance levels from 103 to 11 μmol photons m^{-2} s^{-1}, respectively (Supporting Information Table S3).

Coral collections and abundance

At each site, coral cover was assessed visually by the scientific collector viewing an area ~ 5 m^2 around the site of coral collection via a submersible window (Fig. 1). Representative corals approximately 20–30 cm in diameter were haphazardly selected from the middle of *Leptoseris* reefs, with each sample separated by at least 10 m from other samples. A small, triangular piece of coral from the middle to the outer edge of each coral head was removed using a Schilling Titan 4 manipulator arm (Fig. 1C) and placed in an individual sample container in the sampling basket. After collection, samples were placed in a darkened container with ambient seawater at in situ seawater temperatures and processed in a darkened, air conditioned laboratory, using red light headlamps with an intensity of ~ 1 μmol photons m^{-2} s^{-1} from a distance of 40–50 cm, onboard the R/V *Ka'imikai-O-Kanaloa* within 3–9 h of ascent. Two sets of coral samples were collected. One sample set was analyzed for photosynthetic potential, host genetics, *Symbiodinium* genetics, *Symbiodinium* density, photosynthetic pigments, and total lipids. A second set of samples from different coral colonies was collected for isotopic analyses. It is important to note that the second set of samples did not include genetic analyses for host and *Symbiodinium* identification (Supporting Information Table S1). Sample size for physiological and photobiological analyses differed due to sample and instrumentation availability and is reported for each parameter in the sections below. Supporting Information Table S1 includes the location and date of all collections with the physiological and photobiological analyses performed on each sample. After collecting and assessing photosynthetic potential (in the first set of coral samples), fragments were frozen using dry ice and maintained in a –80°C freezer until analyzed.

Laboratory analysis

Pulse amplitude-modulated fluorometry

Photosynthetic potential was assessed with modulated chlorophyll fluorescence measurements taken with a pulse amplitude-modulated (PAM) fluorometer and a red (650 nm) excitation beam (Diving-PAM). A 2-cm-long piece of black tubing (1 cm diameter) was attached to the PAM fiber optic sensor to standardize the area measured and to ease the placement of the sensor onto the coral surface. Actinic PAR values from the Diving-PAM with the fiber optic sensor tubing were calibrated with a cosine underwater quantum sensor (LI-COR LI-192SA) and data logger (LI-COR LI-1400). Measurements of minimum (F_o) and maximum (F_m) fluorescence were used to calculate variable ($F_v = F_m/F_o$) fluorescence and subsequently the maximum quantum yield of photosystem II (PSII) fluorescence (F_v/F_m) or the number of functional photosynthetic units (Ralph and Gademann 2005). To account for potential spatial variation in coral physiology, ~ 10 measurements of F_v/F_m were taken from haphazardly selected, spatially separated points on the coral tissue surface and averaged for each sample (n = 57 coral colonies). Rapid light response curves (RLC) were then taken to measure photosynthetic potential under different light levels following Ralph and Gademann (2005). Each RLC exposed the coral to eight incremental steps of irradiance, similar to the local environment, from 0 to 75 μmol photons m^{-2} s^{-1}. This lower range of irradiances was used on corals from all depths to avoid photoinhibition in corals from deeper depths. Irradiances were set to provide sufficient measurement steps ~ 4–5 measuring points below

saturation, for accurate initial slope (α) calculations. The electron transport rate (ETR) at each irradiance was calculated using the formula ETR = $F_v/F_m \times$ PAR $\times$ 0.5, where the quantum yield is the parameter measured at each irradiance of PAR, and 0.5 is the theoretical distribution of absorbed photons between PSII and photosystem I (PSI), although this balance was not evaluated for these samples. Average ETRs by actinic irradiances for each algal sample were fit to a three-parameter nonlinear model as described by Ralph and Gademann (2005). RLC data were used to estimate the relative maximum ETR ($rETR_{max}$), α (initial slope of the RLC), and the light saturation coefficient (E_k). We used the relative measure of rETR because the exact absorbance of the coral is unknown and likely varies by species and depth-related skeletal phenotypic differences. Curves were fit using the Regression Wizard in Sigmaplot (v. 12.0, SPSS), and estimates of $rETR_{max}$, α, and E_k were used for analyses. In all samples, the model fits the data well with an r^2 of 0.97 $\pm$ 0.01 (mean $\pm$ SEM).

Algal pigments

Algal pigments were extracted as previously described in Padilla-Gamiño et al. (2013). Briefly, glass fiber filters (0.7 μm pore size, GF/F; Whatman) containing the coral and algal tissue homogenate (n = 75) were extracted in 3 mL of high-performance liquid chromatography–grade acetone in glass culture tubes along with 50 μL of an internal standard (canthaxanthin) at 4°C in the dark for 24 h. The extracts were processed following Bidigare et al. (2005); pigments were detected with a ThermoSeparation Products UV2000 detector (λ_1 = 436, λ_2 = 450). Concentrations of photosynthetic (chlorophyll *a* [Chl *a*], Chl c_2, and peridinin) and photoprotective (β-carotene, dinoxanthin, diadinoxanthin, and diatoxanthin) pigments and ratios at the colony and algal cellular level were computed by normalizing to coral surface area (μg pigment cm^{-2}) and *Symbiodinium* density (pg pigment $cell^{-1}$). Our study did not attempt to differentiate the sources of Chl *a* among *Symbiodinium* and endolithic algae. Approximately 85% of the coral skeletons had visible endoliths; 71% of the skeletons had green endoliths; and 23% had both green and orange endoliths. To minimize endolithic contribution in the pigment extractions, we only used homogenate derived from coral tissue (not skeleton). Identities of pigments produced exclusively by dinoflagellate symbionts (i.e., peridinin and Chl *c*; Kleppel et al. 1989) show proportions or similar patterns to our Chl *a* data suggesting that our pigment quantification mostly represented extracts from *Symbiodinium* (Supporting Information Fig. S2).

***Symbiodinium* densities**

The densities and size of *Symbiodinium* cells were examined according to Apprill et al. (2007). In brief, coral tissue (n = 75) was removed from the frozen fragment using a Waterpik® and filtered seawater (FSW, 0.2 μm). The homogenate tissue was then blended for 30 s and centrifuged for 5 min. Multiple washing steps were performed with FSW to ensure the complete separation of *Symbiodinium* and coral tissue. The *Symbiodinium* suspensions were analyzed using a Beckman-Coulter XL flow cytometer with a 15-mW argon ion laser set to excite at 488 nm. The flow cytometer was interfaced with an Orion syringe pump for quantitative sample analysis using a 3 mL syringe delivering 100 μL of suspended cells at a flow rate of 50 μL min^{-1} for measurement of fluorescence emission of Chl *a* (630 nm dichroic filter, 680 nm bandpass filter), as well as forward and side scatter signals. Duplicate abundance estimates were averaged for each sample. *Symbiodinium* abundances were standardized to coral surface area measured with the aluminum foil method (Marsh 1970). Symbiont subpopulations were identified based on side scatter (cell size) and fluorescence characteristics. Listmode files generated by the Flow cytometer were analyzed using FlowJo software (Treestar) by species. The number of symbionts from each symbiont subpopulation for each individual was quantified using FlowJo software and converted to the percent distribution of the three subpopulations and graphically represented using a ternary diagram (SigmaPlot 13.0 ©2014, Systat Software; Supporting Information Fig. S3).

Coral and *Symbiodinium* genetics

Host and *Symbiodinium* genotypes of our samples (except samples used for isotopic signatures) were reported previously in Pochon et al. (2015) and examined using coral (*COX1-1-rRNA* intron) and *Symbiodinium* (*COI*) mitochondrial markers (n = 74). Generally, *COI* haplotypes corresponded with specific *ITS2* community sequence profiles. Haplotype *COI-1* was uniquely associated with *ITS2* sequence type C1v18, haplotype *COI-2* was associated with *ITS2* sequence types C1v1d and C1c/C45, and haplotype *COI-3* was associated with *ITS2* sequence types C1v1b, C1v1c, C1v3, and C1v8 (Pochon et al. 2012). However, *ITS2* sequence types C1 and C1v1e were associated with all *COI* haplotypes, and *ITS2* sequence type C1v6 was associated with both *COI-1* and *COI-2* (Pochon et al. 2015).

Total lipids and biomass

Total lipids and biomass (n = 75) were obtained following Rodrigues and Grottoli (2007). In brief, ground coral samples were extracted in a 2 : 1 chloroform : methanol solution, the organic phase was then washed using 0.88% KCl, and the lipid extract dried to a constant weight. Tissue biomass was estimated using the difference between dry weight and ash free dry weight. Lipids and biomass were normalized to surface area.

Stable isotopes

Coral tissue and *Symbiodinium* were removed from skeletons using a WaterPik with FSW (n = 21–25; Johannes and Wiebe 1970). Host and *Symbiodinium* fractions were separated using a centrifuge that isolated zooxanthellae as a pellet. Pellets were washed and resuspended using FSW, then centrifuged, repeating the procedure twice. To ensure separation,

pellets and supernatant were examined periodically under a microscope. Both resuspended pellets and supernatant were separately collected on a precombusted GF/F filter using vacuum filtration. Filtered fractions were analyzed for elemental and isotopic composition of carbon and nitrogen ($\delta^{13}C$ = ratio of ^{13}C : ^{12}C relative to Vienna Peedee Belemnite Limestone Standard and $\delta^{15}N$ = ratio of ^{15}N : ^{14}N relative to air, reported in permil units) using an elemental analyzer coupled to a Thermo Delta V isotope ratio mass spectrometer. When ample material was present, sample analyses were duplicated. A subset of samples was acidified on the filter to test for residual skeletal material. Acidification showed no indication of skeletal contamination with replicate standard deviations averaging 0.2‰ for *Symbiodinium* (C and N) and 0.3‰ and 0.8‰ for C and N, respectively.

Statistical analyses

Independent data analyses for each species were grouped based on a depth-dependent light gradient: 70 m (~ 55 μmol photons m^{-2} s^{-1}, 65–75 m), 80 m (~ 36 μmol photons m^{-2} s^{-1}, 76–85 m), 90 m (~ 24 μmol photons m^{-2} s^{-1}, 86–95 m), 100 m (~ 16 μmol photons m^{-2} s^{-1}, 96–105 m), and 120 m (~ 10–5 μmol photons m^{-2} s^{-1}, 115–125 m). Physiological values of *Leptoseris papyracea* were not included in any of the statistical analyses associated with depth because the species was found at only one depth range (90 m). Comparisons of physiological traits between species were performed using a one-way analysis of variance (ANOVA). Prior to analyses, data were normalized as necessary using logarithmic or square root transformations to achieve homogeneity of variances and normality. Homogeneity of variance and normality was assessed using Shapiro–Wilk W and Levene tests, respectively. When significant effects were identified, Tukey's post hoc tests were performed to determine differences between depths. Statistical differences were significant at the $\alpha < 0.05$ level. Wilcoxon-Signed Rank Tests were performed when normality was not achieved after transformation. Data are represented as mean ± SEM. We did not perform ANOVA analyses for isotopic signatures because genetic information was not available for this subset of samples, instead the relationship between isotopic signature and depth in *Leptoseris* spp. was assessed using linear regressions. Statistical analyses were performed using JMP version 12.2.0 (SAS Institute).

Results

Leptoseris spp. complex depth distribution

Cryptically diverse species of *Leptoseris* were present between 60 and 132 m; however, coral cover and diversity of species (host and *Symbiodinium*) varied across depths (Figs. 1–2). The lowest coral cover was found between 70 and 80 m (~ 36–55 μmol photons m^{-2} s^{-1}; Fig. 1) with only *Leptoseris* sp. 1, *Leptoseris tubulifera*, and *Leptoseris scabra* present (Fig. 2). At shallow depths (70–80 m), *Symbiodinium* spp. *COI-2* and *COI-3* haplotypes were nearly equally abundant, making up 60% and 40% of the population, respectively (Fig. 2). The highest coral cover and highest diversity in *Leptoseris* spp. occurred between 90 and 100 m (Figs. 1–2). At these depths, irradiance (~ 16–24 μmol photons m^{-2} s^{-1}) corresponded to 1–2% of the irradiance just below the surface (1066 μmol photons m^{-2} s^{-1})

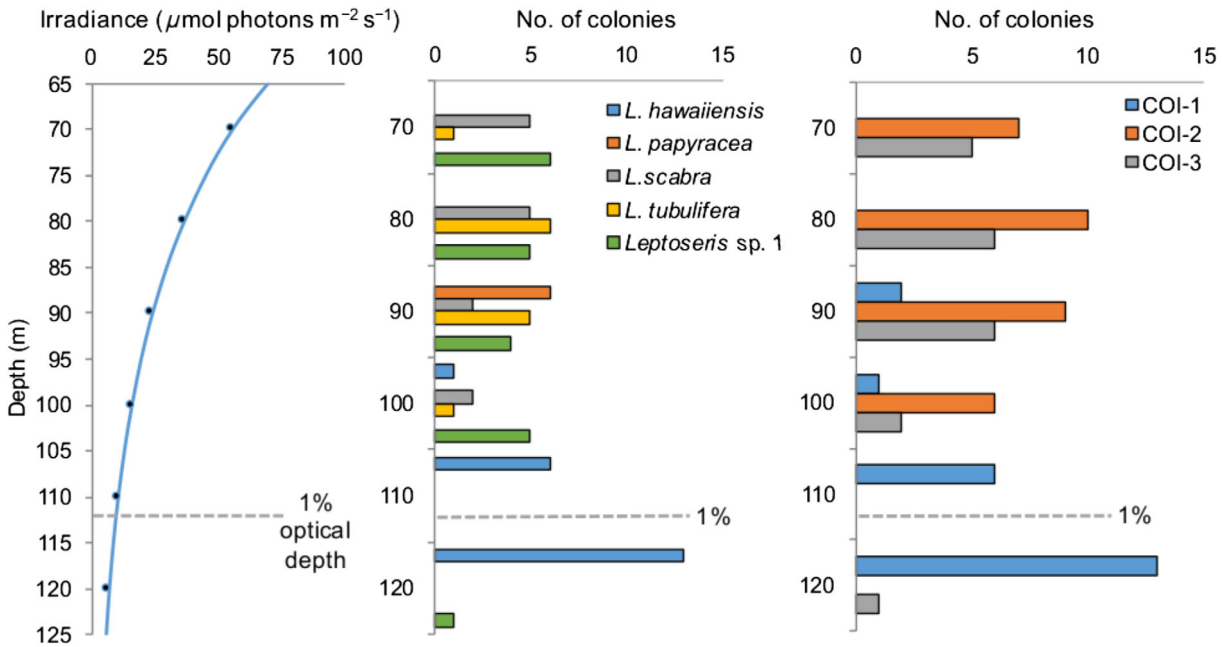

Fig. 2. Irradiance in the 'Au'au Channel, Hawai'i, and distribution of *Leptoseris* spp. and *Symbiodinium* spp. *COI* haplotypes by collection depths (from Pochon et al. 2015).

during summer months in 2008 and 2010 (Fig. 2; Supporting Information Table S2 and S3). Similarly, the highest diversity in *Symbiodinium* occurred between 90 and 100 m with all haplotypes present (Fig. 2). At the deepest depths (110–120 m or ~ 10–16 μmol photons m^{-2} s^{-1}; Fig. 1E–F), coral cover was around 20–35% and *L. hawaiiensis* was the dominant species, although sporadic colonies of *Leptoseris* sp. 1 were present (Figs. 1–2). The deepest locations (110–120 m) had the lowest symbiont diversity; *Symbiodinium* spp. *COI-1* was the dominant symbiont present in 100% and 93% of the samples at 110 and 120 m, respectively (Fig. 2). The lower depth of *L. hawaiiensis* and *Leptoseris* sp. 1 was observed at 125 m (Fig. 2), indicating that these species live beyond the expected 1% surface values and at irradiances as low as 5.2 μmol photons m^{-2} s^{-1}.

Photophysiological specialization of *Leptoseris* spp. across depth

L. scabra

Our data suggest that *L. scabra* is a broadly shade-tolerant species, adjusting subcellular photosynthetic components to maintain optimal performance with decreasing PAR and depth. Photosynthetic and accessory pigments in *L. scabra* increased with depth ($p < 0.05$; Fig. 3; Supporting Information Table S4) allowing colonies to maintain ETR_{max}. Chl *a* cm^{-2} concentrations at 70 m were only 28% of the pigment concentrations at 100 m depth (0.43 and 1.53 μg cm^{-2}, respectively; Supporting Information Table S4). Therefore, surface area for light harvesting is the most important factor limiting the depth distribution of this species. Despite being found across a wide depth range (70–100 m), *L. scabra* did not exhibit significant changes in other photophysiological variables across depths, such as pigments per cell, pigment ratios, *Symbiodinium* cell size (Fig. 3; Supporting Information Table S4), dark-adapted quantum yield, maximum rETR, or E_k ($p > 0.05$; Fig. 4). Similarly, lipid content did not change with depth in *L. scabra* or any of the other *Leptoseris* spp. (Supporting Information Table S4). *L. scabra* showed very similar physiological characteristics to *L. tubulifera* including close association with *Symbiodinium* haplotype *CO1-2,* high tissue biomass, small-size *Symbiodinium*, and higher β-carotene : Chl *a* ratios compared to the other *Leptoseris* spp. (Table 1).

Leptoseris sp. *1*

In contrast to *L. scabra*, *Leptoseris* sp. 1 was found across a wider depth range (70–120 m) and exhibited changes in *Symbiodinium* haplotype (*CO1* and *CO2*) with depth (Pochon et al. 2015) that may have influenced the photobiological response and coral acclimatization capacity with depth. *Symbiodinium* density significantly increased with depth in *Leptoseris* sp. 1, with ~ 58% higher *Symbiodinium* densities at 100 m than at 70 m (3.3×10^5 and 5.69×10^5 cells cm^{-2}; 70 and 100 m, respectively; Fig. 3; Supporting Information Table S4). Similarly, Chl *c* : Chl *a* ratios increased with depth (Fig. 3). Dark-adapted quantum yield remained constant across depths, while $rETR_{max}$ and E_k increased at 80 m depth ($F = 3.993$, $p = 0.0415$; $F = 6.367$, $p = 0.011$, $rETR_{max}$ and E_k respectively; Fig. 4; Supporting Information Table S4). Physiological characteristics of *Leptoseris sp.* 1 were more closely related to *L. scabra* and *L. tubulifera* than *L. hawaiiensis*; however, *Leptoseris sp.* 1

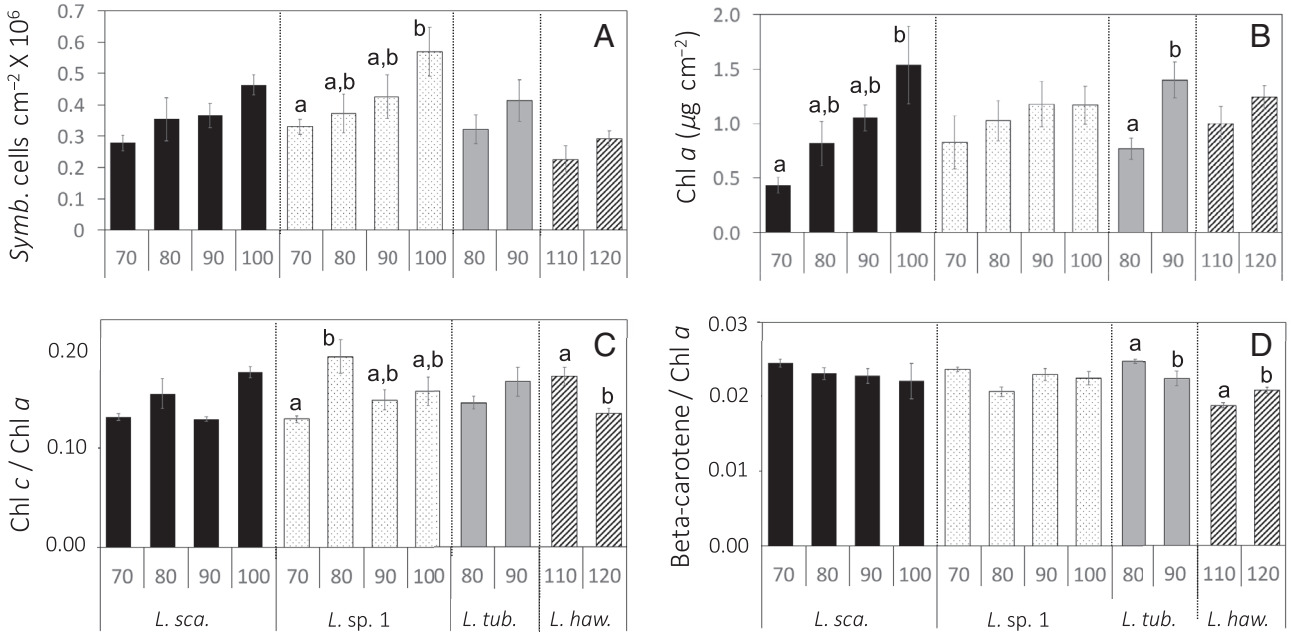

Fig. 3. (**A**) *Symbiodinium* density, (**B**) Chl *a* (μg cm^{-2}), (**C**) Chl *c* : Chl *a,* and (**D**) β-carotene in four species of *Leptoseris* spp. in Hawai'i. *L. sca, scabra* (black); *L.* sp. 1, *Leptoseris* sp. 1 (dots); *L. tub, L. tubulifera* (gray); and *L. haw., L. hawaiiensis* (diagonal).

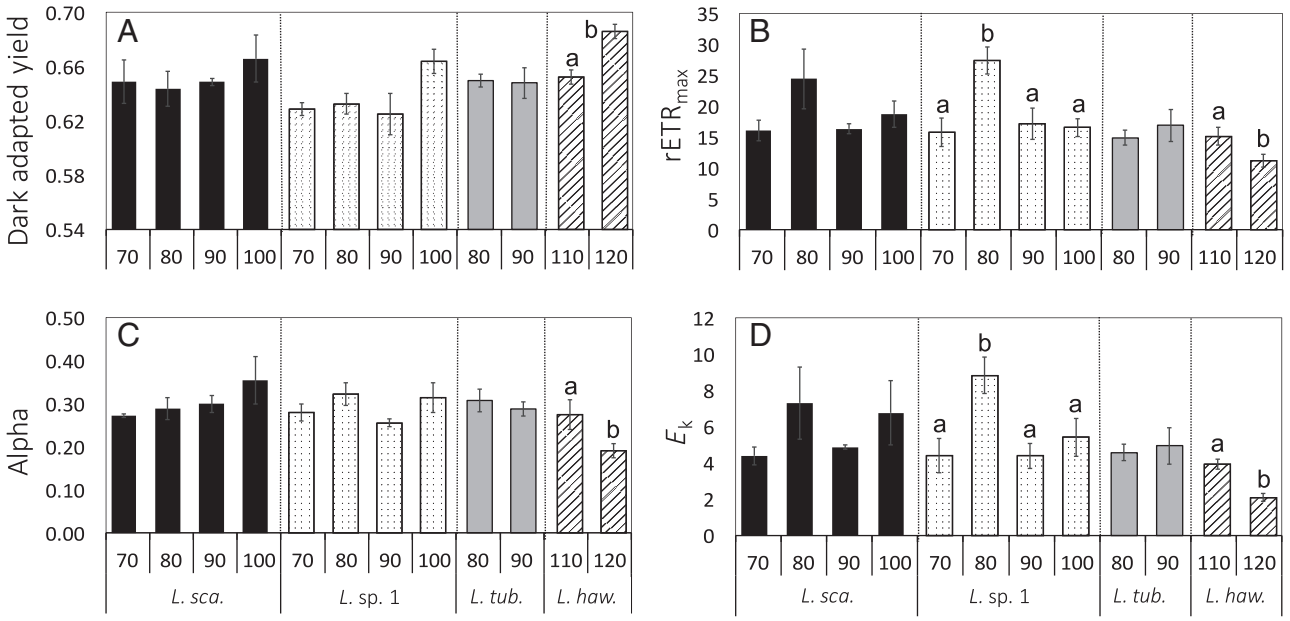

Fig. 4. (**A**) Dark-adapted quantum yield, (**B**) maximum relative ETR, (**C**) α, and (**D**) E_k in *Leptoseris* spp. in Hawai'i. *L. sca*, *scabra* (black); *L.* sp. 1, *Leptoseris* sp. 1 (dots); *L. tub*, *L. tubulifera* (gray); and *L. haw.*, *L. hawaiiensis* (diagonal).

had larger *Symbiodinium* cells than either *L. scabra* or *L. tubulifera* (Table 1). Finally, *Leptoseris* sp. 1 and *L. payracea* had the highest *Symbiodinium* densities of all species (Table 1).

L. tubulifera

Similar to *L. scabra*, *L. tubulifera* showed an increase in pigment concentrations with depth ($p < 0.05$; Fig. 3; Supporting Information Table S4) to maintain optimal performance with decreasing PAR and depth; with Chl *a* cm^{-2} increasing ~ 55% from 80 to 90 m (0.77 to 1.40 μg cm^{-2}, respectively; Fig. 3). Although *L. scabra* was present from 70 to 100 m, we excluded samples from 70 and 100 m in the statistical analyses due to low sample size. Not surprisingly, between 80 and 90 m, there was no significant change in photosynthetic pigments normalized by cell, lipids, dark-adapted quantum yield, maximum rETR$_{max}$, or E_k ($p > 0.05$; Figs. 3–4; Supporting Information Table S4). However, β-carotene : Chl *a* decreased ~ 8% from 80 to 90 m depth (Fig. 3). Physiological trends in *L. tubulifera* were very similar to *L. scabra* (see above; Table 1) most likely due to their shared association with *Symbiodinium* haplotype *CO1-2*.

L. papyracea

L. papyracea was very abundant within a narrow depth range (86–95 m, ~ 24 μmol photons m^{-2} s^{-1}). This species was deep-shade adapted showing the highest Chl *c* : Chl *a* and *Symbiodinium* densities (~ 0.18 and 0.59 × 106, respectively) and the lowest lipid values (211 mg cm^{-2}) among all *Leptoseris* species ($p < 0.05$; Table 1). Despite their narrow range, *L. papyracea* colonies at 87 m were strictly associated with *Symbiodinium* haplotype *COI-3*, whereas *L. papyracea* colonies at 95 m only hosted *Symbiodinium* haplotype *COI-1* (Pochon et al. 2015).

L. hawaiiensis

L. hawaiiensis lives at depths with the lowest irradiance levels (110–120 m, 10–5 μmol photons m^{-2} s^{-1}, respectively) and below the threshold-value of the lower limit of the euphotic zone (i.e., at 112 m there is less than 1% surface irradiance). Yet *Symbiodinium* (*COI-1*) in these colonies still exhibit classic shade adaptation. At 120 m, *Symbiodinium* cell size decreased ~ 6% compared to *Symbiodinium* cells at 110 m ($p = 0.011$, $F = 6.475$; Fig. 3). Chl *c* : Chl *a* and DDX + DTX : Chl *a* ratios also decreased (24% and 2%, respectively, $p = 0.004$, $F = 8.377$; $p = 0.044$, $F = 4.069$) at 120 m, whereas β-carotene : Chl *a* ratios increased 10% (Fig. 3; $p = 0.011$, $F = 6.469$; Supporting Information Table S4). Dark-adapted quantum yield increased at 120 m ($F = 15.604$, $p = 0.001$; Fig. 4), whereas rETR$_{max}$, E_k, and α decreased at this depth (Fig. 4; $p < 0.05$; Supporting Information Table S4). Compared to other species, *L. hawaiiensis* showed the lowest *Symbiodinium* densities and the largest Chl *a* content per cell (Fig. 4; Table 1). The relative total xanthophyll pool, β-carotene : Chl *a* ratios, and tissue biomass were the lowest in *L. hawaiiensis* compared to other *Leptoseris* spp. (Fig. 3; Table 1); however, lipid content (mg cm^{-2}) was the highest (Table 1). Fluorescence parameters showed a very distinct response in *L. hawaiiensis*; this species had the lowest rETR$_{max}$, α, and E_k and the highest values of dark-adapted yields compared to other species of *Leptoseris* (Fig. 4; Table 1).

Leptoseris spp. *complex isotopic signatures*

Carbon isotopic composition of *Symbiodinium* ranged from −21.9‰ to −18.9‰ and from −19.1‰ to −22.7‰ in hosts, with similar means in both fractions (−20.3‰ and −20.9‰,

Table 1. Physiological differences among *Leptoseris* spp. in Hawai'i.

Species	*L. scabra*	*Leptoseris* sp. *1*	*L. tubulifera*	*L. papyracea*	*L. hawaiiensis*
Depth range (m)	**70–100**	**70–100**	**70–100***	**90**	**110–120**
***Symbiodinium* haplotype**	***COI-2***	***COI-2* and *COI-3***	***COI-2***	***COI-1* and *COI-3***	***COI-1***
Biomass (mg cm^{-2})	17.33 ± 12.3 $^{(A)}$	11.73 ± 7.1 $^{(A)}$	14.51 ± 7.5 $^{(A)}$	9.04 ± 2.4 $^{(A,B)}$	7.17 ± 2.7 $^{(B)}$
Lipids (mg cm^{-2})	413.91 ± 334.4 $^{(B)}$	581.77 ± 319.3 $^{(C,B)}$	425.45 ± 257.6 $^{(A, B)}$	211.22 ± 154.6 $^{(A)}$	845.42 ± 417.3 $^{(C)}$
Symbiodinium cells cm^{-2}	0.34 ± 0.1 $^{(B,C)}$	0.41 ± 0.2 $^{(A,B)}$	0.36 ± 0.1 $^{(B,C)}$	0.59 ± 0.2 $^{(A)}$	0.27 ± 0.1 $^{(C)}$
Cell size (mm)	8.81 ± 0.3 $^{(A)}$	9.54 ± 0.6 $^{(B)}$	8.78 ± 0.2 $^{(A)}$	9.25 ± 0.5 $^{(B)}$	9.19 ± 0.6 $^{(A,B)}$
Chl *a* (mg cm^{-2})	0.82 ± 0.5 ^{ns}	1.05 ± 0.5 ^{ns}	1.09 ± 0.4 ^{ns}	1.14 ± 0.4 ^{ns}	1.19 ± 0.2 ^{ns}
Dinoxanthin (mg cm^{-2})	0.02 ± 0.01 $^{(A)}$	0.03 ± 0.01 $^{(A,B)}$	0.02 ± 0.01 $^{(A,B)}$	0.03 ± 0.01 $^{(A, B)}$	0.03 ± 0.01 $^{(B)}$
Chl *a* (pg cell^{-1})	2.29 ± 1.0 $^{(A)}$	2.72 ± 1.3 $^{(A)}$	3.22 ± 1.3 $^{(A, B)}$	1.93 ± 0.4 $^{(A)}$	4.71 ± 2.0 $^{(B)}$
Chl *c*/Chl *a*	0.15 ± 0.03 $^{(A)}$	0.15 ± 0.03 $^{(A)}$	0.15 ± 0.02 $^{(A)}$	0.18 ± 0.02 $^{(B)}$	0.15 ± 0.03 $^{(A)}$
DDX + DTX/Chl *a*	0.13 ± 0.004 $^{(C)}$	0.13 ± 0.005 $^{(A)}$	0.13 ± 0.005 $^{(A, B)}$	0.13 ± 0.001 $^{(B,C)}$	0.12 ± 0.122 $^{(D)}$
Beta-carotene/Chl *a*	0.023 ± 0.002 $^{(A)}$	0.022 ± 0.002 $^{(A)}$	0.024 ± 0.002 $^{(A)}$	0.020 ± 0.001 $^{(B)}$	0.018 ± 0.002 $^{(B)}$
Dark-adapted yield	0.65 ± 0.02 $^{(A)}$	0.65 ± 0.03 $^{(A)}$	0.65 ± 0.02 $^{(A, B)}$	0.64 ± 0.02 $^{(A)}$	0.67 ± 0.02 $^{(B)}$
$rETR_{max}$	5.70 ± 2.3 $^{(A)}$	5.74 ± 2.7 $^{(A)}$	4.62 ± 1.1 $^{(A)}$	6.97 ± 1.2 $^{(A)}$	2.96 ± 1.4 $^{(B)}$
Alpha	0.30 ± 0.05 $^{(A)}$	0.29 ± 0.06 $^{(A)}$	0.30 ± 0.04 $^{(A)}$	0.33 ± 0.04 $^{(A,B)}$	0.23 ± 0.08 $^{(B)}$
E_k	18.88 ± 5.7 $^{(A)}$	19.07 ± 6.3 $^{(A)}$	15.38 ± 3.0 $^{(A,B)}$	21.15 ± 3.8 $^{(A)}$	13.14 ± 4.39 $^{(B)}$

Numbers in the table represent averages and standard deviations for each species including all depths. Significant differences between species are represented by superscripts.
DDX, diadinoxanthin; DTX, diatoxanthin.

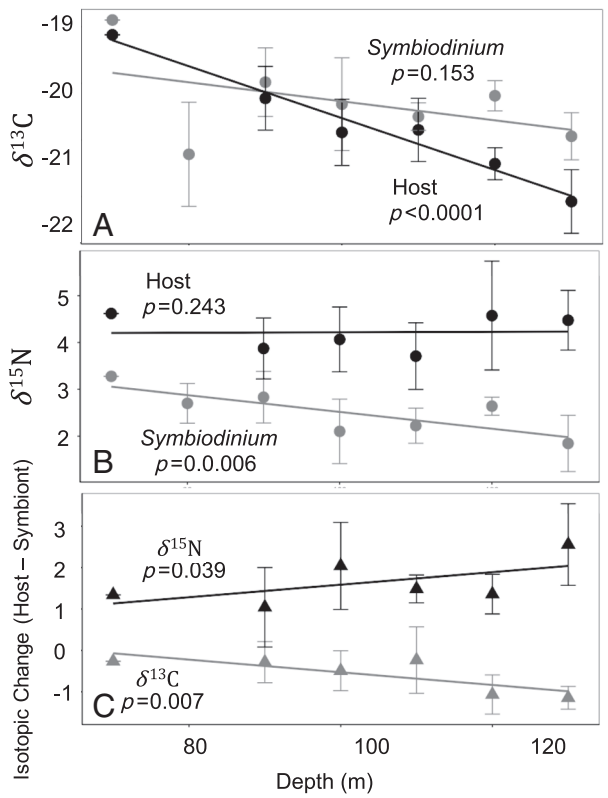

Fig. 5. (**A**) δ^{13}C, (**B**) δ^{15}N signatures, and translocation between host and *Symbiodinium* of *Leptoseris* spp. at different depths. (**A**, **B**) Coral host fraction in black and *Symbiodinium* fraction in gray, and (**C**) difference between animal and *Symbiodinium*, δ^{13}C (gray) and δ^{15}N (black). Means and standard deviations are plotted; lines represent linear regressions for host and *Symbiodinium*.

respectively). Host δ^{13}C values decreased linearly with increasing depth ($p < 0.0001$, $F = 49.5$; Fig. 5A). However, *Symbiodinium* δ^{13}C values did not show a significant trend with depth. Bulk stable isotopic values for nitrogen in *Symbiodinium* ranged from 1.1‰ to 3.4‰, whereas that of the host tissue ranged from 2.7‰ to 6.3‰ (mean 2.4‰ and 4.1‰, respectively). *Symbiodinium* δ^{15}N values decreased with increasing depth ($p = 0.008$, $F = 8.69$; Fig. 5B). However, host nitrogen isotopic composition did not show any overall trend with increasing depth ($p = 0.243$). Differences between isotopic composition of coral host and symbiotic algae exhibited dissimilar trends with depth. With increasing depth, *Symbiodinium* became significantly more distinct via changed δ^{15}N compared to host tissue, whereas host tissue became significantly more depleted in δ^{13}C compared to *Symbiodinium* ($p = 0.0397$, $F = 4.83$ and $p = 0.007$, $F = 9.04$, respectively; Fig. 5C). C : N ratios for *Symbiodinium* increased with depth ($p = 0.025$) and ranged from 5.7 to 9.5 (mean = 6.9), whereas C : N ratios for the host decreased with depth ($p = 0.0116$) and ranged from 5.5 to 16.75 (mean = 7.79).

Discussion

In this study, we explore the depth-dependent variability in trophic strategies, photophysiological, and genetic traits of four *Leptoseris* spp. Our robust, cross-cutting approach revealed different physiological strategies used by the algae and coral species to obtain energy and persist in a deep-shade environments. This work uncovered three fundamental insights into coral–algal symbiosis, photophysiology, and trophic plasticity

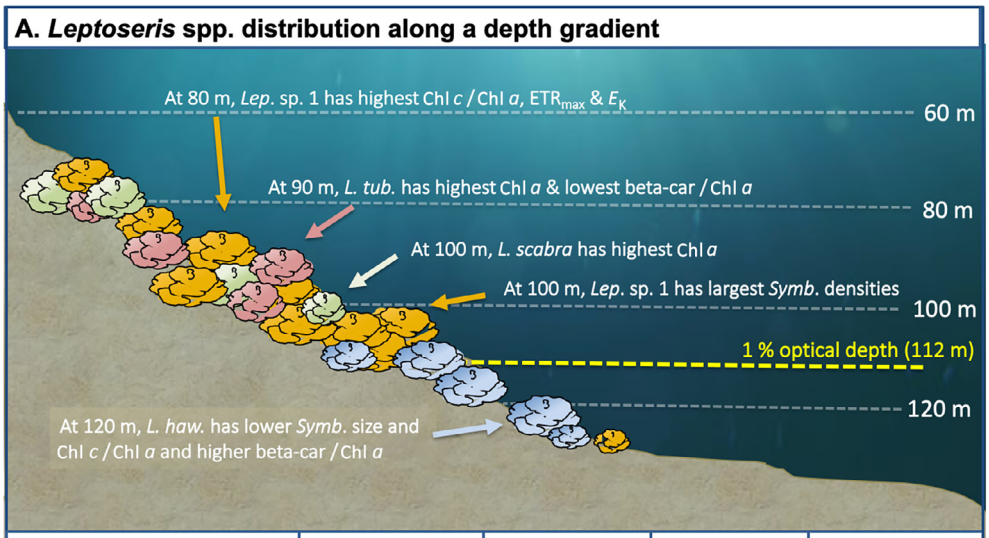

B. Physiological trends with depth by *Leptoseris* species	*Leptoseris* sp.1	*L. tubulifera*	*L. scabra*	*L. hawaiiensis*
Depth range	**70-100**	**70-100**	**70-100**	**110-120**
Symbiodinium type	COI-3 & COI-2	COI-2	COI-2	COI-1
Symbiodinium cells cm^{-2}	↑	-	-	-
Cell size	-	-	-	↓
Chl *a* (μg cm^{-2})	-	↑	↑	-
Chl *c* / Chl *a*	↑@ 80 m	-	-	↓
DDX+DTX / Chl *a*	-	-	-	↓
Beta-carotene / Chl *a*	-	↓	-	↑
Dark-adapted yield	-	-	-	↑
rETRmax	↑@ 80 m	-	-	↓
Alpha	-	-	-	↓
E_k	↑@ 80 m	-	-	↓
PHOTOCHEMISTRY	ETR: 80 m, 70, 90, 100 m; PAR	ETR: No difference 70-100 m; PAR	ETR: No difference 70-100 m; PAR	ETR: 110 m, 120 m; PAR

Fig. 6. Schematic representing (**A**) *Leptoseris* spp. distribution along a depth gradient and (**B**) physiological trends with depth. "-," no difference in the physiological variable across depth.

in mesophotic environments. To begin, plasticity of *Leptoseris*–algal photophysiology across depths was associated with the type of *Symbiodinium* spp. Colonies harboring *Symbiodinium* spp. *COI-2* (*L. tubulifera* and *L. scabra*) showed significant increases in photosynthetic pigment content with increasing depth but no change in chlorophyll fluorescence with depth (Fig. 6), suggesting a complex that is broadly tolerant to its depth conditions. In contrast, colonies harboring *Symbiodinium* spp. *COI*-1 or *COI-3* (*L. hawaiiensis* and *Leptoseris* sp. 1) showed variability in pigment ratios, chlorophyll fluorescence, and *Symbiodinium* density and/or size (Fig. 6), suggesting that flexibility in photoacclimatization as well as photoadaptation among these *Leptoseris*–algal complexes depends primarily on *Symbiodinium* genotypes. Furthermore, despite remarkable differences in photosynthetic adaptive strategies with depth, we found no differences in total lipid content of *Leptoseris* spp. species over the same depth range (Supporting Information Table S4). This finding suggests that photosynthetic acclimatization with depth resulted in similar acquisition and translocation of lipids to the hosts and/or hosts may be supplementing their total lipid reserves from nonphotosynthetic sources at deeper depths. Finally, isotopic

signatures of both host and *Symbiodinium* changed with depth supporting the lipid findings and indicating that coral colonies may acquire energy from different sources along their depth gradient. Overall, our results show marked complexity in physiological adaptations of species in the *Leptoseris* spp. complex and highlight the diversity of strategies used to acquire energy and succeed in environments where irradiance is extremely limited.

Photophysiology

Because mesophotic reef-building corals live close to the limits of the depth distribution for Scleractinian corals, their photophysiology is likely to reveal novel acclimatization and adaptation strategies in photosynthetic symbioses. Our results show that *Leptoseris* species have different host–*Symbiodinium* specializations and physiological plasticity along a depth gradient. *L. scabra* and *L. tubulifera* were almost exclusively associated with *Symbiodinium* spp. *COI-2* haplotype but showed the ability to increase *Symbiodinium* pigment concentrations (per surface area) with depth. This pattern is similar to *M. cavernosa* in the mesophotic Caribbean (Lesser et al. 2010), but the opposite trend was observed for *L. fragilis* in the mesophotic Red Sea (Fricke et al. 1987; Schlichter et al. 1997). *L. tubulifera*, however, showed greater phenotypic variation in symbiont populations (Supporting Information Fig. S3) and lower β-carotene : Chl *a* with increasing depths, suggesting that this species has more diverse *Symbiodinium* (type, size, quantum yield, or cell division rates) and that β-carotene has primarily a photoprotective function at shallower depths.

Leptoseris sp. 1 (70–100 m) was the only species that increased *Symbiodinium* density with depth. Colonies of this species at 100 m had twice the density of *Symbiodinium* than colonies at 70 m. Increased *Symbiodinium* density under low light conditions has been observed in the field experimentally in *Stylophora pistillata* (Dubinsky and Jokiel 1994; Titlyanov et al. 2001). Under light-limited conditions (~ 8% surface irradiance), light harvesting in *S. pistillata* was maximized by an increase in *Symbiodinium* density, which was primarily regulated by division and degradation of *Symbiodinium* cells (Titlyanov et al. 2001). Thus, it is likely that increased *Symbiodinium* density may facilitate photosynthetic energy acquisition of *Leptoseris* sp. 1 at deeper depths. Nutrients have also been associated with increased densities of *Symbiodinium* (Sawall et al. 2014); however, the nutrient dynamics in the mesophotic region and the role of nutrient limitation or enrichment in the ecophysiology of *Leptoseris* spp. in the mesophotic zone remains unknown. Conversely, *Symbiodinium* densities of *L. fragilis* in the mesophotic zone of the Red Sea decreased ~ 50% between 100 and 130 m (Fricke et al. 1987) and *Symbiodinium* densities decreased in colonies of the genera *Leptoseris*, *Pachyseris*, *Seriatopora*, *Porites*, and *Podabacia* from 1 to 60 m depths in Australia and the Red Sea (Cooper et al. 2011; Ziegler et al. 2015).

The increase in *Symbiodinium* densities with depth in *Leptoseris* sp. 1 was not associated with changes in Chl *a* cm^{-2} or *Symbiodinium* size. However, Chl *c* : Chl *a* showed an increase with depth (70 to 80 m), indicating photoacclimatization by increasing light harvesting antennae to gather light and augment light energy capture to the photosynthetic reaction center (Roth et al. 2010). Additionally, at shallow depths (70–80 m), *Leptoseris* sp. 1 was strictly associated with *Symbiodinium* haplotype *COI-3*, whereas at deeper depths colonies were associated with *Symbiodinium* haplotypes *COI-2* and *COI-3* (Pochon et al. 2015). Thus, it is likely that the differences in photosynthetic pigment content, composition, and *Symbiodinium* density are not only the result of photobiological adaptation but also the result of strong selective pressures on the interactions between the hosts and their different *Symbiodinium* assemblages (Baker 2003) to optimize light harvesting at these remarkable depths.

Strikingly, *L. hawaiiensis* was the dominant species below the 1% optical depth where irradiance levels are lower than 1% of the surface irradiance. This species exhibited a highly-specialized association with *Symbiodinium* haplotype *COI-1*, which had the highest variability in photobiology with depth compared to other species within the *Leptoseris* complex. In this species, dark-adapted yield increased with depth, whereas values for $rETR_{max}$, α, and E_k declined with depth. At the deepest depth range (115–125 m), we found lower rates of photosynthetic electron transport and unexpectedly lower efficiency at subsaturating irradiances (α). Similar results were found in *M. cavernosa* (Lesser et al. 2010), where $rETR_{max}$ and gross primary productivity decreased with depth (3–90 m depth range). For *L. hawaiiensis*, *Symbiodinum* size and Chl *c* : Chl *a* decreased with depth, suggesting genetic or energetic limitations on cell parameters and/or the amounts of pigments that can be produced. This could enforce less reliance on light capture for carbon gain by the host.

Photoprotective pigments had different patterns with depth in *L. hawaiiensis*. As expected, the relative xanthophyll pool : Chl *a* pool decreased with depth. However, β-carotene in *L. hawaiiensis* increased with depth, indicating that it is more likely to play a role as a structural component of the light-harvesting complex rather than as a photoprotective pigment. Further research including collections in different seasons is necessary to quantify the physiological flexibility of *Leptoseris* spp. over larger temporal scales and examine whether pigment composition and relative abundance change as light becomes more available with higher sun declination and longer day length. It is important to note that *L. hawaiiensis* photosynthesizes in a habitat with approximately half of the light available (~ 6 μmol photons m^{-2} s^{-1}) at the 1% surface irradiance. This is a remarkable system that warrants further photosynthetic research and a re-evaluation of our understanding of the mechanisms that set lower limits of the euphotic zone and the strategies evolved by these endemic species to persist in these environments.

This study reveals remarkable species differentiation by *Symbiodinium* and *Leptoseris* under extreme light limitation in the mesophotic zone including changing pigment quantities and composition, photochemistry parameters, and/or *Symbiodinium*

type, density and size. Chlorophyll fluorescence RLC measurements should be interpreted with caution given the caveats and assumptions involved with data collection and interpretation (Warner et al. 2010). The RLC data should not be confused with traditional oxygen-based photosynthesis to irradiance (P–E) curves, and cannot be used to infer total photosynthetic productivity. Absorption was not measured in this study but was assumed to be about 1, given the lower light environment and likely maximized light harvesting found at 65 to 125 m depths. Measurements of *M. cavernosa* absorbance had similar values ranging from 0.951 ± 0.010 to 0.963 ± 0.012 from 45 to 91 m depths, respectively (Lesser et al. 2009). Future studies should involve simultaneous measurements of photosynthesis and ETR, detailed absorbance and reflectance measurements, and the role of endolithic green algae in influencing the spectral signal of mesophotic corals. The use of a modified ETR equation that uses the spectral reflectance of the coral surface where fluorescence measurements are recorded and then converted to the absorbance band at 675 nm (Enríquez et al. 2005) would also be useful for comparison for future studies.

Another aspect to consider is that morphological, physiological, and behavioral adaptations may also occur in the host to control and optimize light acquisition (Maxwell and Johnson 2000). In response to light, corals can modify skeletal morphology (Muko et al. 2000; Enríquez et al. 2005; Todd 2008), produce antioxidants and fluorescent proteins (Muko et al. 2000; Enríquez et al. 2005; Todd 2008), and change tissue thickness, polyp size, density, and behavior (Porter 1976; Fitt et al. 2000; Levy et al. 2003; Wangpraseurt et al. 2014). In Hawai'i, *Leptoseris* in the mesophotic zone exhibits flatter morphologies with increasing depth (Kahng et al. 2012; J.L.P.-G. personal observation), nonphotosynthetic fluorescent pigments are found in the host throughout its depth range (Porter 1976; Fitt et al. 2000; Levy et al. 2003; Wangpraseurt et al. 2014), and skeletal design and structures maximize light scatter through the coral tissue (Kahng et al. 2012; Kahng 2014). The upper side of *Leptoseris* skeletons has ordered rows of concave cavities that increase the probability of light scattering to maximize light capture (Kahng et al. 2012; Kahng 2014).

Energy reserves and acquisition

Despite dynamic changes in photophysiology, total host lipids were not significantly different across depths, suggesting that lipid acquisition is maintained by nonphotosynthetic sources at some depths. As shown by Muscatine et al. (1989) and observed here for *Leptoseris* spp. (Fig. 5), the more rapid depletion of ^{13}C in host tissue of *Leptoseris* spp. compared to *Symbiodinium* indicates that animal tissue at depth incorporates carbon from other sources, including heterotrophy and/or dissolved organic carbon, in addition to photosynthesis. Moreover, the relative similarity of carbon isotopic composition between host and *Symbiodinium* at the shallowest depths suggests that heterotrophic inputs do not become significant until well into the mesophotic realm (120–130 m). Similar patterns were observed in *M. cavernosa* in the Caribbean where $\delta^{13}C$ values of host and *Symbiodinium* only differed at the deepest collection site (91 m), suggesting less translocation of photosynthates to the host and larger dependency by the host cells on heterotrophy and/or other sources of carbon at depth (Lesser et al. 2010).

The *Leptoseris* spp. complex consists of several cryptic species (Pochon et al. 2015); however, species data were not available for the isotopic samples presented (Fig. 5; Supporting Information Table S1). Therefore, it is possible that the stable carbon isotopic patterns that we observed in host and symbiont across depth may be the result of differences in heterotrophic plasticity as previously described (Muscatine et al. 1989) or differences in lipid production and storage among species, as lipids typically lower the $\delta^{13}C$ values of host tissue (Deniro and Epstein 1977; Alamaru et al. 2009). Although we cannot confirm the species analyzed in the isotopic samples, our study suggest that greater differences in $\delta^{13}C$ across depth between host and symbiont tissues are more likely influenced by preferential reliance on heterotrophic sources at depth than differences in storage or production of lipid content between species (Supporting Information Table S4; Fig. 6). This is further supported by C : N depth-patterns in host and *Symbiodinium*. Lower C : N ratios in the host at deeper depths indicate higher nitrogen content from heterotrophic activity and/or less carbon translocated to the host by *Symbiodinium* due to lower light levels at depth and increased nitrogen limitation (Dubinsky and Jokiel 1994).

The $\delta^{15}N$ values were higher in the host than in *Symbiodinium* at all depths. This trend is consistent with previous observations in *M. cavernosa* (Muscatine and Kaplan 1994; Lesser et al. 2010), *S. pistillata* and *Favia favus* (Alamaru et al. 2009). Enriched stable nitrogen isotopic signatures in the host may be attributable to protein catabolism and excretion of isotopically light ammonium (Deniro and Epstein 1977; Alamaru et al. 2009) and/or metabolic fractionation related to changes in trophic level (Muscatine and Kaplan 1994). Because corals use the products of photosynthesis by *Symbiodinium*, an isotopic enrichment in the host is expected.

In *Symbiodinium*, $\delta^{15}N$ values decreased with depth, whereas host $\delta^{15}N$ values remained constant across depths (Fig. 5). Muscatine and Kaplan (1994) found a similar trend of depth-related depletion of $\delta^{15}N$ in *Symbiodinium* of several species of Jamaican scleractinian corals that corresponded to decreasing nitrogen-specific growth rates in deeper waters. Likewise, the *Symbiodinium* of *S. pistillata* and *F. favus* decreased with depth, whereas the host tissue remained the same across depth (Alamaru et al. 2009). The mesophotic depths in the 'Au'au Channel correspond to the seasonal thermocline in that region (Pyle et al. 2016), which may serve as a location for turbulent mixing and upwelling of deep nutrients. During the warmer months (September–November), however, the thermocline is strongest (Pyle et al. 2016) and during this period vertical

mixing of nutrients from below may be limited. This pattern of ^{15}N depletion in the symbiont tissue with depth, while there is no change in host tissue, is expected if corals are primarily feeding on isotopically heavier allochthonous sources of particulate organic matter (POM) at mesophotic depths (> 100 m).

In *L. fragilis,* POM feeding is possible because their gastrovascular system works like a filtration system. Water flow enters through the mouth of *L. fragilis* and leaves the body through microscopic pores in the oral epithelia. Moreover, nematocysts are abundant and present in this species (Schlichter 1991), suggesting that feeding by predation of microzooplankton could be another important strategy for nutrient acquisition in *Leptoseris* from Hawai'i. Further research is necessary to fully characterize the gastrovascular system in this species and examine the isotopic signature of zooplankton and POM in the mesophotic zone; this will help to better understand the heterotrophic capacity of this important genus across depths.

Conclusions

Species of *Leptoseris* in the mesophotic zone in Hawai'i have different associations with dinoflagellate symbionts that can contribute to the colony's capacity to acquire energy photoautotrophically. Our results show that the distribution of these species is a consequence of host–*Symbiodinium* specialization, physiological plasticity as well as photoadaptation across species. However, species living at deeper depths also showed a capacity to acquire energy heterotrophically, possibly by filter feeding (Schlichter 1991) and/or feeding on detritus and/or dissolved organic matter as reflected by no change in total lipid concentrations across depth and supported by differences between host and *Symbiodinium* isotopic values. These findings serve as a foundation to study physiological flexibility in the mesophotic zone and help us to better understand the ecology and resilience of these understudied but highly important native ecosystems.

References

Alamaru, A., Y. Loya, E. Brokovich, R. Yam, and A. Shemesh. 2009. Carbon and nitrogen utilization in two species of Red Sea corals along a depth gradient: Insights from stable isotope analysis of total organic material and lipids. Geochim. Cosmochim. Acta **73**: 5333–5342. doi:10.1016/j.gca.2009.06.018

Apprill, A., R. Bidigare, and R. Gates. 2007. Visibly healthy corals exhibit variable pigment concentrations and symbiont phenotypes. Coral Reefs **26**: 387–397. doi:10.1007/s00338-007-0209-y

Baker, A. C. 2003. Flexibility and specificity in coral-algal symbiosis: Diversity, ecology, and biogeography of *Symbiodinium*. Annu. Rev. Ecol. Evol. Syst. **34**: 661–689. doi:10.1146/annurev.ecolsys.34.011802.132417

Baker, E. K., and P. T. Harris. 2016. Mesophotic coral ecosystems: A lifeboat for coral reefs? United Nations Environment Programme and GRID-Arendal.

Bidigare, R. R., L. Van Heukelem, and C. C. Trees. 2005. Analysis of algal pigments by high-performance liquid chromatography. Algal culturing techniques. Academic Press.

Bongaerts, P., T. Ridgway, E. Sampayo, and O. Hoegh-Guldberg. 2010. Assessing the 'deep reef refugia' hypothesis: Focus on Caribbean reefs. Coral Reefs **29**: 309–327. doi:10.1007/s00338-009-0581-x

Bouchon, C. 1981. Quantitative study of the scleractinian coral communities of a fringing reef of Reunion Island (Indian Ocean). Mar. Ecol. Prog. Ser. **4**: 273–288. doi:10.3354/meps004273

Brazeau, D. A., M. P. Lesser, and M. Slattery. 2013. Genetic structure in the coral, *Montastraea cavernosa*: Assessing genetic differentiation among and within mesophotic reefs. PLoS One **8**: e65845. doi:10.1371/journal.pone.0065845

Bridge, T. C., T. J. Done, A. Friedman, R. J. Beaman, S. B. Williams, O. Pizarro, and J. M. Webster. 2011. Variability in mesophotic coral reef communities along the great barrier reef, Australia. Mar. Ecol. Prog. Ser. **428**: 63–75. doi:10.3354/meps09046

Bryan, D. R., K. Kilfoyle, R. G. Gilmore, and R. E. Spieler. 2013. Characterization of the mesophotic reef fish community in South Florida, USA. J. Appl. Ichthyol. **29**: 108–117. doi:10.1111/j.1439-0426.2012.02055.x

Cooper, T. F., and others. 2011. Niche specialization of reef-building corals in the mesophotic zone: Metabolic trade-offs between divergent *Symbiodinium* types. Proc. R. Soc. Lond. B Biol. Sci. **278**: 1840–1850. doi:10.1098/rspb.2010.2321

Costa, B., and others. 2015. Identifying suitable locations for mesophotic hard corals offshore of Maui, Hawai 'i. PLoS One **10**: e0130285. doi:10.1371/journal.pone.0130285

Deniro, M. J., and S. Epstein. 1977. Mechanism of carbon isotope fractionation associated with lipid synthesis. Science **197**: 261–263. doi:10.1126/science.327543

Dubinsky, Z., and P. L. Jokiel. 1994. Ratio of energy and nutrient fluxes regulates symbiosis between zooxanthellae and corals. Pac. Sci. **48**: 313–324. http://hdl.handle.net/10125/2241

Enríquez, S., E. R. Méndez, and R. Iglesias-Prieto. 2005. Multiple scattering on coral skeletons enhances light absorption by symbiotic algae. Limnol. Oceanogr. **50**: 1025–1032. doi:10.4319/lo.2005.50.4.1025

Falkowski, P. G., and J. A. Raven. 2007. Aquatic photosynthesis. Princeton Univ. Press.

Fitt, W., F. Mcfarland, M. Warner, and G. Chilcoat. 2000. Seasonal patterns of tissue biomass and densities of symbiotic dinoflagellates in reef corals and relation to coral bleaching. Limnol. Oceanogr. **45**: 677–685. doi:10.4319/lo.2000.45.3.0677

Frade, P., N. Englebert, J. Faria, P. Visser, and R. Bak. 2008. Distribution and photobiology of *Symbiodinium* types in different light environments for three colour morphs of the coral

Madracis pharensis: Is there more to it than total irradiance? Coral Reefs **27**: 913–925. doi:10.1007/s00338-008-0406-3

Fricke, H. W., and H. Schuhmacher. 1983. The depth limits of Red Sea stony corals: An ecophysiological problem (a deep diving survey by submersible). Mar. Ecol. **4**: 163–194. doi:10.1111/j.1439-0485.1983.tb00294.x

Fricke, H. W., and B. Knauer. 1986. Diversity and spatial pattern of coral communities in the Red Sea upper twilight zone. Oecologia **71**: 29–37. doi:10.1007/BF00377316

Fricke, H. W., E. Vareschi, and D. Schlichter. 1987. Photoecology of the coral *Leptoseris fragilis* in the Red Sea twilight zone (an experimental study by submersible). Oecologia **73**: 371–381. doi:10.1007/BF00385253

Gattuso, J.-P., B. Gentili, C. M. Duarte, J. Kleypas, J. J. Middelburg, and D. Antoine. 2006. Light availability in the coastal ocean: Impact on the distribution of benthic photosynthetic organisms and contribution to primary production. Biogeosci. Discuss. **3**: 895–959. doi:10.5194/bgd-3-895-2006

Goreau, T. F., and N. I. Goreau. 1959. The physiology of skeleton formation in corals. II. Calcium deposition by hermatypic corals under various conditions in the reef. Biol. Bull. **117**: 239–250. doi:10.2307/1538903

Hinderstein, L. M., J. C. A. Marr, F. A. Martinez, M. J. Dowgiallo, K. A. Puglise, R. L. Pyle, D. G. Zawada, and R. Appeldoorn. 2010. Theme section on "Mesophotic coral ecosystems: Characterization, ecology, and management", v. **29**. Springer.

Hoadley, K. D., and others. 2015. Physiological response to elevated temperature and pCO_2 varies across four Pacific coral species: Understanding the unique host+ symbiont response. Sci. Rep. **5**: 18371. doi:10.1038/srep18371

Holstein, D. M., C. B. Paris, A. C. Vaz, and T. B. Smith. 2016. Modeling vertical coral connectivity and mesophotic refugia. Coral Reefs **35**: 23–37. doi:10.1007/s00338-015-1339-2

Johannes, R. E., and W. J. Wiebe. 1970. Method for determination of coral tissue biomass and composition. Limnol. Oceanogr. **15**: 822–824. doi:10.4319/lo.1970.15.5.0822

Kahng, S. E. 2013. Growth rate for a zooxanthellate coral (*Leptoseris hawaiiensis*) at 90 m. Galaxea J. Coral Reef Stud **15**: 39–40. doi:10.3755/galaxea.15.2_39

Kahng, S. E. 2014. Unlocking the secrets of Hawaii's deep-water photosynthetic corals. Reef Encounter **29**: 19–22.

Kahng, S. E., and J. E. Maragos. 2006. The deepest, zooxanthellate scleractinian corals in the world? Coral Reefs **25**: 254–254. doi:10.1007/s00338-006-0098-5

Kahng, S. E., and C. Kelley. 2007. Vertical zonation of megabenthic taxa on a deep photosynthetic reef (50–140 m) in the Au'au Channel, Hawaii. Coral Reefs **26**: 679–687. doi:10.1007/s00338-007-0253-7

Kahng, S. E., E. J. Hochberg, A. Apprill, D. Wagner, D. G. Luck, D. Perez, and R. R. Bidigare. 2012. Efficient light harvesting in deep-water zooxanthellate corals. Mar. Ecol. Prog. Ser. **455**: 65–77. doi:10.3354/meps09657

Kane, C., R. K. Kosaki, and D. Wagner. 2014. High levels of mesophotic reef fish endemism in the northwestern Hawaiian islands. Bull. Mar. Sci. **90**: 693–703. doi:10.5343/bms.2013.1053

Kirk, J. T. 2011. Light and photosynthesis in aquatic ecosystems. Cambridge Univ. Press.

Kleppel, G., R. E. Dodge, and C. Reese. 1989. Changes in pigmentation associated with the bleaching of stony corals. Limnol. Oceanogr. **34**: 1331–1335. doi:10.4319/lo.1989.34.7.1331

Leal, M. C., K. Hoadley, D. T. Pettay, A. Grajales, R. Calado, and M. E. Warner. 2015. Symbiont type influences trophic plasticity of a model cnidarian–dinoflagellate symbiosis. J. Exp. Biol. **218**: 858–863. doi:10.1242/jeb.115519

Lesser, M. P., M. Slattery, and J. J. Leichter. 2009. Ecology of mesophotic coral reefs. J. Exp. Mar. Biol. Ecol. **375**: 1–8. doi:10.1016/j.jembe.2009.05.009

Lesser, M. P., M. Slattery, M. Stat, M. Ojimi, R. D. Gates, and A. Grottoli. 2010. Photoacclimatization by the coral *Montastraea cavernosa* in the mesophotic zone: Light, food, and genetics. Ecology **91**: 990–1003. doi:10.1890/09-0313.1

Levy, O., Z. Dubinsky, and Y. Achituv. 2003. Photobehavior of stony corals: Responses to light spectra and intensity. J. Exp. Biol. **206**: 4041–4049. doi:10.1242/jeb.00622

Lindfield, S. J., E. S. Harvey, A. R. Halford, and J. L. Mcilwain. 2016. Mesophotic depths as refuge areas for fishery-targeted species on coral reefs. Coral Reefs **35**: 125–137. doi:10.1007/s00338-015-1386-8

Loya, Y., G. Eyal, T. Treibitz, M. P. Lesser, and R. Appeldoorn. 2016. Theme section on mesophotic coral ecosystems: Advances in knowledge and future perspectives. Coral Reefs **35**: 1–9. doi:10.1007/s00338-016-1410-7

Luck, D. G., Z. H. Forsman, R. J. Toonen, S. J. Leicht, and S. E. Kahng. 2013. Polyphyly and hidden species among Hawai'i's dominant mesophotic coral genera, *Leptoseris* and *Pavona* (Scleractinia: Agariciidae). PeerJ **1**: e132. doi:10.7717/peerj.132

Maragos, J. E., and P. L. Jokiel. 1986. Reef corals of Johnston atoll: One of the world's most isolated reefs. Coral Reefs **4**: 141–150. doi:10.1007/BF00427935

Marsh, J. A. 1970. Primary productivity of reef-building calcareous red algae. Ecology **51**: 255–263. doi:10.2307/1933661

Maxwell, K., and G. N. Johnson. 2000. Chlorophyll fluorescence—A practical guide. J. Exp. Bot. **51**: 659–668. doi:10.1093/jexbot/51.345.659

Muko, S., K. Kawasaki, K. Sakai, F. Takasu, and N. Shigesada. 2000. Morphological plasticity in the coral *Porites sillimaniani* and its adaptive significance. Bull. Mar. Sci. **66**: 225–239.

Mundy, C., and R. Babcock. 1998. Role of light intensity and spectral quality in coral settlement: Implications for depth-dependent settlement? J. Exp. Mar. Biol. Ecol. **223**: 235–255. doi:10.1016/S0022-0981(97)00167-6

Muscatine, L. 1990. The role of symbiotic algae in carbon and energy flux in reef corals, p. 75–87. *In* Ecosystems of the world, v. **25**. Amsterdam, The Netherlands: Elsevier Science Publishing Company, Inc.

Muscatine, L., P. Falkowski, Z. Dubinsky, P. Cook, and L. Mccloskey. 1989. The effect of external nutrient resources on the population dynamics of zooxanthellae in a reef coral. Proc. R. Soc. Lond. B Biol. Sci. **236**: 311–324. doi:10.1098/rspb.1989.0025

Muscatine, L., and I. Kaplan. 1994. Resource partitioning by reef corals as determined from stable isotope composition II. $\delta^{15}N$ of zooxanthellae and animal tissue versus depth. Pac. Sci. **48**: 304–312. http://hdl.handle.net/10125/2240

Padilla-Gamiño, J. L., and others. 2013. Are all eggs created equal? A case study from the Hawaiian reef-building coral *Montipora capitata*. Coral Reefs **32**: 137–152. doi:10.1007/s00338-012-0957-1

Pernice, M., and others. 2015. A nanoscale secondary ion mass spectrometry study of dinoflagellate functional diversity in reef-building corals. Environ. Microbiol. **17**: 3570–3580. doi:10.1111/1462-2920.12518

Pochon, X., H. M. Putnam, F. Burki, and R. D. Gates. 2012. Identifying and characterizing alternative molecular markers for the symbiotic and free-living dinoflagellate genus *Symbiodinium*. PLoS One **7**: e29816. doi:10.1371/journal.pone.0029816

Pochon, X., Z. Forsman, H. Spalding, J. Padilla-Gamiño, C. Smith, and R. Gates. 2015. Depth specialization in mesophotic corals (*Leptoseris* spp.) and associated algal symbionts in Hawai'i. R. Soc. Open Sci. **2**: 140351. doi:10.1098/rsos.140351

Porter, J. W. 1976. Autotrophy, heterotrophy, and resource partitioning in Caribbean reef-building corals. Am. Nat. **110**: 731–742. doi:10.1086/283100

Pyle, R. L., and others. 2016. A comprehensive investigation of mesophotic coral ecosystems in the Hawaiian archipelago. PeerJ **4**: e2475. doi:10.7717/peerj.2475

Ralph, P. J., and R. Gademann. 2005. Rapid light curves: A powerful tool to assess photosynthetic activity. Aquat. Bot. **82**: 222–237. doi:10.1016/j.aquabot.2005.02.006

Riegl, B., and W. E. Piller. 2003. Possible refugia for reefs in times of environmental stress. Int. J. Earth Sci. **92**: 520–531. doi:10.1007/s00531-003-0328-9

Rodrigues, L. J., and A. G. Grottoli. 2007. Energy reserves and metabolism as indicators of coral recovery from bleaching. Limnol. Oceanogr. **52**: 1874–1882. doi:10.4319/lo.2007.52.5.1874

Rooney, J., and others. 2010. Mesophotic coral ecosystems in the Hawaiian archipelago. Coral Reefs **29**: 361–367. doi:10.1007/s00338-010-0596-3

Roth, M. S. 2014. The engine of the reef: Photobiology of the coral–algal symbiosis. Front. Microbiol. **5**: 422. doi:10.3389/fmicb.2014.00422

Roth, M. S., M. I. Latz, R. Goericke, and D. D. Deheyn. 2010. Green fluorescent protein regulation in the coral *Acropora yongei* during photoacclimation. J. Exp. Biol. **213**: 3644–3655. doi:10.1242/jeb.040881

Sawall, Y., A. Al-Sofyani, E. Banguera-Hinestroza, and C. R. Voolstra. 2014. Spatio-temporal analyses of *Symbiodinium* physiology of the coral Pocillopora verrucosa along large-scale nutrient and temperature gradients in the Red Sea. PLoS One **9**: e103179. doi:10.1371/journal.pone.0103179

Schlichter, D. 1991. A perforated gastrovascular cavity in *Leptoseris fragilis*. Naturwissenschaften **78**: 467–469. doi:10.1007/BF01134387

Schlichter, D., W. Weber, and H. Fricke. 1985. A chromatophore system in the hermatypic, deep-water coral *Leptoseris fragilis* (Anthozoa: Hexacorallia). Mar. Biol. **89**: 143–147. doi:10.1007/BF00392885

Schlichter, D., H. Kampmann, and S. Conrady. 1997. Trophic potential and photoecology of endolithic algae living within coral skeletons. Mar. Ecol. **18**: 299–317. doi:10.1111/j.1439-0485.1997.tb00444.x

Shlesinger, T., M. Grinblat, H. Rapuano, T. Amit, and Y. Loya. 2018. Can mesophotic reefs replenish shallow reefs? Reduced coral reproductive performance casts a doubt. Ecology **99**: 421–437. doi:10.1002/ecy.2098

Spalding, H. L., K. Y. Conklin, C. M. Smith, C. J. O'kelly, and A. R. Sherwood. 2016. New Ulvaceae (Ulvophyceae, Chlorophyta) from mesophotic ecosystems across the Hawaiian archipelago. J. Phycol. **52**: 40–53. doi:10.1111/jpy.12375

Spalding, H. L., and others. 2018. Mesophotic coral ecosystems in Hawaii. *In* K. Puglise, Y. Loya, and T. C. L. Bridge [eds.], Coral reefs of the world: Mesophotic ecosystems. Springer.

Titlyanov, E., T. Titlyanova, K. Yamazato, and R. Van Woesik. 2001. Photo-acclimation dynamics of the coral *Stylophora pistillata* to low and extremely low light. J. Exp. Mar. Biol. Ecol. **263**: 211–225. doi:10.1016/S0022-0981(01)00309-4

Todd, P. A. 2008. Morphological plasticity in scleractinian corals. Biol. Rev. **83**: 315–337. doi:10.1111/j.1469-185X.2008.00045.x

Veazey, L. M., E. C. Franklin, C. Kelley, J. Rooney, L. N. Frazer, and R. J. Toonen. 2016. The implementation of rare events logistic regression to predict the distribution of mesophotic hard corals across the main Hawaiian islands. PeerJ **4**: e2189. doi:10.7717/peerj.2189

Wangpraseurt, D., A. W. Larkum, J. Franklin, M. Szabó, P. J. Ralph, and M. Kühl. 2014. Lateral light transfer ensures efficient resource distribution in symbiont-bearing corals. J. Exp. Biol. **217**: 489–498. doi:10.1242/jeb.091116

Warner, M. E., M. P. Lesser, and P. J. Ralph. 2010. Chlorophyll fluorescence in reef building corals, p. 209–222. *In* Chlorophyll a fluorescence in aquatic sciences: Methods and applications. Springer.

Ziegler, M., C. M. Roder, C. Büchel, and C. R. Voolstra. 2015. Mesophotic coral depth acclimatization is a function of host-specific symbiont physiology. Front. Mar. Sci. **2**: 4. doi:10.3389/fmars.2015.00004

Acknowledgments

We thank the Hawai'i Undersea Research Laboratory (HURL) *Pisces V* submersible and *RCV-150* pilots, crew, and support staff, as well as the crew of the R/V *Ka'imikai-o-Kanaloa*, for access to these amazing depths. This article includes results of research funded by the National Oceanic and Atmospheric Administration (NOAA) Center for Sponsored Coastal Ocean Research (Coastal Ocean Program) under award to the Bishop Museum, NA07NOS4780187 and NA07NOS478190 to the University of Hawai'i and NA07NOS4780189 to the State of Hawai'i; submersible support provided by NOAA Undersea Research Program's Hawai'i HURL; and funding from the NOAA Coral Reef Conservation Program research grants program administered by HURL under award NA09OAR4300219, project number HC08-06. Physiological analyses were funded by grants from the National Science Foundation (NSF) Experimental Program to Stimulate Competitive Research (EPSCoR, EPS-0903833) and Bio Oce (OCE-0752604) both awarded to R.D.G. and by Villanova University to L.J.R. Work by J.L.P.-G. was supported by NSF (IOS-1655682 awarded to J.L.P.-G.) and work by M.S.R. was supported by the Division of Chemical Sciences, Geosciences, and Biosciences, Office of Basic Energy Sciences, Office of Science, U.S. Department of Energy, FWP number 449B, and the Agriculture and Food Research Initiative Competitive Grant 2013-67012-21272 from the USDA National Institute of Food and Agriculture. Coral samples were collected under SAP permit 2009-72 from the Department of Land and Natural Resources, State of Hawai'i. However, the majority of corals was collected in U.S. Federal Waters and did not require a permit for collection. We thank F. Parrish for use of fluorescence NightSea equipment; B. Popp, A. Grottoli, J. Rooney, and K. Binsted for assistance in collecting and processing samples during the cruise; T. M. Weatherby, T. S. Christensen, F. Butler, and K. Selph for assistance in processing samples after the cruise; and K. Puglise for overall support of the project. This is the School of Ocean and Earth Science and Technology contribution 10662 and Hawaii Institute of Marine Biology Contribution 1754.

Author contribution statement

J.L.P.-G. and H.L.S. conceived, designed, and coordinated the study; J.L.P.-G. drafted the manuscript; J.L.P.-G., H.L.S., and M.S.R. collected field data; J.L.P.-G., H.L.S., L.J.R., and C.J.B. carried out statistical and physiological analyses; J.L.P.-G., H.L.S., M.S.R., L.J.R., C.J.B., R.R.B., R.D.G., and C.M.S. wrote the manuscript. All authors gave final approval for publication.

Conflict of Interest

None declared

Submitted 14 May 2018
Revised 17 December 2018
Accepted 25 February 2019

Associate editor: Núria Marbà